SUBMITTED TO:

Geomechanics for Energy and the Environment

DATE:

26th April 2016

TITLE:

Analysis of Unsaturated Materials Hydration Incorporating the Effect of Thermo-Osmotic Flow

AUTHORS:

Marcelo Sanchez[1], Chloé Arson[2], Antonio Gens[3] Fernando Aponte[1]

AFFILIATIONS:

1. Texas A& M University (TAMU), USA
2. Georgia Institute of Technology (Georgia-Tech), USA
3. Technical University of Catalonia (UPC). Spain

*CORRESPONDING AUTHOR:

Dr Marcelo Sánchez
Associate Professor
Zachry Department of Civil Engineering
Texas A&M University
College Station Texas
77843-3136, USA
Telephone: (+1) 979 862 6604
Fax: (+1) 979 862 7696
E-mail: msanchez@civil.tamu.edu

Keywords: thermo-osmotic flows, unsaturated materials, THM coupled phenomena, compacted expansive clays, nuclear waste disposal, numerical modeling.

ABSTRACT

The geological disposal of a high level radioactive waste relies in a system composed of engineered and geological barriers. The soils and rocks involved in the design of this type of solution are generally initially unsaturated and subject to complex thermal, hydraulic and mechanical (THM) coupled phenomena triggered by the simultaneous heating and hydration of the barrier materials under confined conditions. Mathematical THM formulations are typically used to analyse the behaviour and long term performance of the barriers system. These types of formulations generally do not include some coupled processes, for example thermo-osmosis (i.e. the movement of liquid water induced by gradient of temperature), because they are considered not significant when compared against the main or direct processes (e.g., Darcy's, Fourier's and Fick's laws). In this work the potential effects of thermo-osmotic phenomenon is studied in detail. Typical flow equations are modified to include thermo-osmotic flows and then they are implemented in numerical simulators. Two case studies are analysed. The first one focuses on a simple and already proposed model to study the behaviour of a geological barrier for nuclear waste when subjected to heating and hydration. The other case corresponds to the study of an engineered clay barrier material in the lab subjected to hydraulic and thermal gradients similar to the ones expected in real repository conditions. In both cases the analyses with and without thermo-osmotic flows are compared. From these comparisons it is observed that the effect of thermo-osmosis can be quite significant. Thermo-osmotic effects also assisted to explain the apparent low wetting observed in the hydration of a clayey barrier material.

1. INTRODUCTION

A geological repository for high-level radioactive waste (HLW) disposal is designed to safely contain nuclear waste for a very long period of time. One possible system consists in placing the metallic canisters (containing the nuclear waste) in a network of tunnels excavated in the rock several hundreds of meters (i.e. around 500 m, or more) below the ground level. The empty space between the canister and the drilled gallery is filled with an engineered barrier. The behavior of unsaturated materials is of central interest in the design of HLW repositories due to their potential involvement as: a) raw material to construct the man-made engineered barrier (generally) envisaged around the waste canister; and b) the geological barrier in mined repositories in clay-stone formations.

The engineered barriers are (generally) made up of compacted unsaturated expansive clay has the multiple purposes of providing mechanical stability for the waste canister (for absorbing stresses and deformations); delaying the water flow from the host rock, and providing a suitable chemical environment. The engineered barrier system is a basic element in the design of repository to isolate HLW. It plays a prominent role in conducting the heat generated from the waste; reducing the flow of pore water, and maintaining the structural stability of the waste canister. The barrier undergoes a variety of coupled thermal, hydrological and mechanical (THM) phenomena due to heating (from the heat-emitting nuclear waste); hydration (from the saturated host rock); and constrained volumetric deformations.

Compacted expansive clays in unsaturated state are often used in the design of HLW as sealing material because of, amongst others: their low permeability, swelling properties and self-healing capabilities. Hence current efforts are focused on characterizing the behavior of these clays by conducting experiments (e.g. Push et al.[1], Delage et al.[2], Lloret et al.[3], Villar et al.[4]; Cleall et al.[5,6]), proposing constitutive models (e.g. Gens and Alonso[7], Cui et al.[8], Hueckel and Pellegrini[9], Sanchez et al.[10], François and Laloui[11], Arson and Gatmiri[12], Cleall

et al.[5,6]) and developing mathematical frameworks able to capture the most relevant THM phenomena (e.g. Olivella et al.[13], Rutqvist et al.[14], Gatmiri and Arson[15]).

A good understanding of the non-isothermal behavior of unsaturated materials (i.e. both the compacted clays intended for the engineered barrier, and the host rocks considered for the natural barrier) on the long term basis is necessary for the safe and successful design of the repository. Significant progresses have been made in the last few years in this area. One aspect that still need more attention is the study of the effect of some coupled flow phenomena (that are generally neglected in typical coupled THM analysis) in the long term behavior of HLW repositories. The interest in this type of analysis has increased recently motivated by some apparently unexpected low hydration observed in large scale tests (i.e. Thomas et al.[16], and Sanchez et al.[17]).

This work focuses on the study of the effect of thermo-osmotic flows on the behavior of unsaturated barriers envisioned for HLW disposals. Two case studies are analyzed. The first one is related to a theoretical case proposed by Pollock[16] to study the behavior of a HLW repository in an unsaturated tuff rock. The other one corresponds to the modeling of two infiltration cell experiments, in which both cells are of the same size, but one of them is hydrated under isothermal conditions, and the other is hydrated under a thermal gradient.

The paper is organized as follows: first, the direct and coupled processes typically present in THM coupled analyses in porous media are discussed. Then, the main components of the coupled THM formulation are briefly presented. The case studies are discussed afterwards. The paper closes with the main conclusions of this research.

2. DIRECT AND COUPLED FLOW PROCESSES

Under repository conditions both natural and engineered barriers are subjected to simultaneous thermal, hydraulic, and mechanical phenomena triggered by the heat-emitting nature of the nuclear waste, the water arising from the surrounding rock mass, the swelling

nature of the unsaturated clay barrier, and the highly confined conditions of the isolation system. Coupled THM processes, and their mutual interactions, control the evolution and long-term response of the whole isolation system; therefore, a good understanding of the main THM phenomena is required to achieve a safe design of HLW repositories. Figure 1 schematically illustrates the main physics and their mutual interactions anticipated in a porous medium subjected to simultaneous THM actions. Some of them are discussed in the following.

Within the thermal phenomena, heat storage is assumed to be proportional to temperature. This phenomenon is strongly affected by hydraulic phenomena, via fluid flow; and by the mechanical problem, via porosity changes (which modify the amount of space left for fluids). Phase changes also affect heat storage through the latent heat of vapor. Thermal conductivity is the main property associated with heat conduction that is driven by temperature gradients through Fourier's law. Thermal conductivity depends on partial saturation of the phases and porosity variations (which is related to stress/strain changes). Heat transport in the fluid phases by heat advection (i.e. liquid and gas mass flows) is another important phenomenon related to the thermal problem.

<< Include Figure 1 here>>

Within the hydraulic phenomena, water storage is affected by the thermal problem through the dependence of liquid and vapor density on temperature. Phase change varies the amount of water in liquid and gas phases. Water storage also depends on hydraulic phenomena via the dependence of liquid density on liquid pressure and vapor density on fluid pressures. Water storage is also affected by the mechanical problem through porosity changes. Liquid water transfer is mainly controlled by liquid pressure gradients through Darcy's law. Hydraulic conductivity, is mainly affected by liquid viscosity (which diminishes with temperature); porosity changes (controlled by the mechanical problem); and the degree of

saturation. Furthermore, pore water pressure increases with temperature in saturated and quasi-saturated conditions, and liquid density variation with temperature gives rise to convective flow. Water vapor transfer is mainly controlled by gradients of vapor concentration, i.e. vapor diffusion (through Fick's law) and vapor advection, controlled by gas flow. Vapor diffusion depends mainly on the degree of saturation and porosity changes. Similar processes and couplings govern the air storage, gaseous air transfer and dissolved air transfer.

Within the mechanical phenomena, the mechanical constitutive law establishes the relation between stresses and strains. Temperature field affect the mechanical problem via the thermal expansion/contraction of materials, and the dependence of the constitutive law on temperature. Hydraulic phenomena affect the mechanical field by the dependence of effective or net stresses on fluids pressure. In unsaturated conditions the constitutive laws also depend on suction (i.e. difference between gas and liquid pressures).

Most of the phenomena described above are typically included in standard coupled THM formulations. However, there are additional phenomena in porous media that may be relevant to include in the modeling of certain problems. They are discussed in the following.

The hydraulic gradient is the main physical phenomenon influencing the movement of water in permeable porous media. It is, however, not the only one. Figure 2 presents the main kinds of flow that can occur in a porous media alongside with the corresponding gradient responsible for transport. The word 'law' is generally used for the diagonal terms associated with the direct flow phenomena, and the name 'effect' is reserved to the non-diagonal ones, called also 'coupled processes' (i.e. Bear[19]). Lippmann[20] discovered and named the phenomenon of thermo-osmosis. He discovered it experimentally by separating a volume of water into two parts by means of a membrane. Different temperatures were held in the two

155 regions of the system. The thermal gradient caused a flow of water through the membrane
156 from the cold to the hot side.

157 << Include Figure 2 here>>

158 In permeable reservoirs, the non-diagonal coefficients are relatively small and negligible
159 compared to the diagonal terms. That is the reason why the coupled processes are generally
160 ignored when analyzing problems in aquifers. However, in non-isothermal problems
161 involving low permeability media and/or low hydraulic gradients thermo-osmosis may play a
162 more influential role. Srivastava and Avasthi[21] and Horseman and McEwen[22] showed that
163 water flux due to thermo-osmosis can easily exceed Darcy flux in low permeability clays.
164 The 'phenomenological coefficient' that links each flow with the corresponding driving
165 gradient must be measured experimentally (e.g., Djeran[23]). Accounting for thermo-osmosis
166 implies that the transport of heat may modify the transport of fluids. The counterpart
167 phenomenon of thermo-osmosis is thermo-filtration, which reflects the influence of a
168 pressure gradient on heat flow. Thermo-osmosis and thermo-filtration are generally
169 formulated as reciprocal relations, so that the coupled conductivity terms related to each
170 phenomenon are set equal (Djeran[23]).

171 Thermo-osmotic effects have been studied in the past, for example Soler[24] studied the impact
172 of coupled phenomena on the long-term behavior of radioactive waste repositories in
173 saturated argillaceous rock. Bing Bai[25] proposed an analytical solution in the half-space for
174 the thermal consolidation of layered saturated soils, including the influences of thermo-
175 osmosis and thermal filtration. Chen et al.[26] more recently proposed a coupled THM
176 formulation that accounts for the flow of water and air driven by temperature gradients.

177 The aim of this work is to explore the impact of thermo-osmosis on the hydration of
178 unsaturated soils and rocks generally used in the design of nuclear waste disposals. Thermo-
179 osmosis may have a relevant role during the hydration of barrier materials, especially at

advanced stages when the hydraulic gradient tends to be small and the thermal gradient is still significant (due to the long time involved in the radioactive decay). In this work a standard THM formulation were extended to study the influence of thermo-osmotic flown in coupled THM problems involving unsaturated materials. The main components of a typical THM formulation are presented in the following section together with the incorporation of thermos-osmotic flows

3. MATHEMATICAL FORMULATION

In this section a typical THM formulation to analyze coupled problems in geological media is presented. The general framework is the one proposed by Olivella et al.[27]. The approach is formulated using a multi-phase, multi-species approach. The subscripts identify the phase ('*s*' for solid, '*l*' for liquid and '*g*' for gas). The superscripts indicate the species ('*h*' for mineral, '*w*' for water and '*a*' for air). The liquid phase includes water and dissolved air, and the gas phase is a mixture of dry air and water vapor. Dry air is considered as single species. The framework has three main components: i) balance equations, ii) constitutive laws, and iii) equilibrium conditions. The main components of the mathematical formulation are presented in the following sections, together with the inclusion of the coupled thermo-osmotic flows. More details about the basic formulation can be found elsewhere (i.e. Olivella et al.[13,27]).

3.1 Balance equations

The compositional approach was adopted to establish the mass balance equations, in which balance is expressed for the species rather than the phases. The total mass balance of water is expressed as:

$$\frac{\partial}{\partial t}\left(\theta_l^w S_l n + \theta_g^w S_g n\right) + \nabla \cdot \left(\mathbf{j}_l^w + \mathbf{j}_g^w\right) = f^w \tag{1}$$

where θ_l^w and θ_g^w are the masses of water per unit volume of liquid and gas respectively; n is the porosity; S_l and S_g represent the volumetric fraction of pore volume occupied by liquid

and by gas (degree of saturation for their respective phases); and $\mathbf{j}_l^w$ and $\mathbf{j}_g^w$ denote the total mass fluxes of water in the liquid and gas phases (water vapor), with respect to a fixed reference system. f^w is an external supply of water.

Similarly for the mass balance of air,

$$\frac{\partial}{\partial t}\left(\theta_l^a S_l n + \theta_g^a S_g n\right) + \nabla.\left(\mathbf{j}_l^a + \mathbf{j}_g^a\right) = f^a \tag{2}$$

where $\theta^l{}_a$ and $\theta^g{}_a$ are the masses of air per unit volume of liquid and gas phase respectively. $\mathbf{j}^a{}_l$ and $\mathbf{j}^a{}_g$ denote the total mass fluxes of air in the liquid and gas phases with respect to a fixed reference system. f^a is the external mass supply of air per unit volume of medium.

Thermal equilibrium between phases is assumed. This hypothesis means that at a given material point, the three phases (i.e. solid, liquid and gas) are at the same temperature and, consequently, only one equation is required to establish energy balance. This hypothesis is justified considering the low permeability of the barrier materials. The total internal energy per unit volume of porous media is obtained by adding up the internal energy of each phase. The total internal energy balance equation is expressed as::

$$\frac{\partial}{\partial t}\left(E_s \rho_s (1-n) + E_l \rho_l S_l n + E_g \rho_g S_g n\right) + \nabla.\left(\mathbf{i}_c + \mathbf{j}_{Es} + \mathbf{j}_{El} + \mathbf{j}_{Eg}\right) = f^E \tag{3}$$

where E_s is the solid specific internal energy; E_l and E_g are specific internal energies corresponding to liquid and gas phase, respectively; ρ_s is the solid density; ρ_l and ρ_g are the liquid and gas phase densities; $\mathbf{i}_c$ is the conductive heat flux; $\mathbf{j}_{Es}$ is the advective energy flux of solid phase respect to a fixed reference system; $\mathbf{j}_{El}$ and $\mathbf{j}_{Eg}$ are the advective energy flux of liquid and gas phases, respectively, with respect to a fixed reference system and f^E is the energy supply per unit volume of medium.

The balance of momentum for the porous medium reduces to the equilibrium equation in total stresses:

$$\nabla.\boldsymbol{\sigma}+\mathbf{b}=0 \tag{4}$$

where $\boldsymbol{\sigma}$ is the stress tensor and $\mathbf{b}$ is the vector of body forces. Through an adequate constitutive model (presented in the next section), the equilibrium equation is expressed in terms of solid velocities and fluid pressures. In addition, the mass balance of solid is established for the whole porous medium and it is used to update the porosity.

3.2 Constitutive laws

The constitutive equations establish the link between the main unknowns and the dependent variables. The key constitutive equations are summarized below,

Advective fluxes are computed using a generalized Darcy's law, expressed as:

$$\mathbf{q}_\alpha=-\mathbf{K}_\alpha\left(\nabla P_\alpha-\rho_\alpha\mathbf{g}\right);\qquad \alpha=l,g \tag{5}$$

where P_α is the phase pressure, $\mathbf{K}_\alpha$ is the permeability tensor of α phase and $\mathbf{g}$ is the gravity vector. Specific evolution laws for the permeability law, including intrinsic and relative permeability laws are explained in the case studies.

Non-advective fluxes of species within the fluid phase are related to gradients of mass fraction of species, according to Fick's law. The hydrodynamic dispersion tensor includes both molecular diffusion and mechanical dispersion::

$$\mathbf{i}_\alpha^i=-\mathbf{D}_\alpha^i\nabla\omega_\alpha^i\qquad i=w,a\ ;\quad \alpha=l,g \tag{61}$$

where $\mathbf{D}^i{}_\alpha$ is the dispersion tensor of the medium; a more detailed description of the adopted hydraulic models can be found elsewhere (i.e. Olivella et al.[27]).

Fourier's law describes the conductive flux of heat ($\mathbf{i}_c$) as follows:

$$\mathbf{i}_c=-\lambda\nabla T \tag{7}$$

241 where λ is the thermal conductivity. Specific evolution laws for the thermal conductivity, as
242 well as for other constitutive equations (e.g. water retention curve, mechanical model) are
243 presented together with the application cases.

244 **3.3 Equilibrium restrictions**

245 The equilibrium restrictions control the phase changes. It is assumed that they are rapid in
246 relation to the characteristic times of the flow problems. So, they can be considered in local
247 equilibrium, giving rise to a set of equilibrium restrictions that must be satisfied at all times.
248 The vapor concentration in the gaseous phase is governed by the psychometric law and the
249 amount of air dissolved in water is given by Henry's law (Olivella et al.[27]).

250 **3.4 Thermo-osmotic flow**

251 Philip and de Vries[28] early investigated thermal effects in unsaturated soils. Their model takes
252 into account capillary effects. It also considers the possible presence of air in the soil. With
253 this background, several approaches were proposed to model unsaturated soil behavior:
254 among others: Milly[29], Olivella et al.[27], Gatmiri and Arson[15]. In such approaches, the
255 geomaterial behavior is generally described using a multiphase/multispecies mathematical
256 formulation and assuming that the perfect gas law rule is valid to model the behavior of the
257 gas phase (as described above). Phase changes add some complexity to the problem.
258 Evaporation and condensation may occur under the combined influence of pressure and
259 temperature. As a result, a porous medium filled with a mixture of liquid water and gaseous
260 air in fact also encompasses vapor. Water flow thus depends on liquid water and on vapor
261 transfers. The vapor term may encompass temperature gradients modeling either the
262 vaporization process, or the behavior of a perfect gas.
263 This study is aimed at extending existent THM formulations (like the ones cited above, which
264 only consider the laws in the diagonal of Figure 2) to include thermo-coupled processes

induced by thermal gradients. The constitutive models for the thermo-osmosis can be obtained by adding a conductivity term multiplying the gradient of temperature in the generalized Darcy's equation (i.e. Eq. 5). Put in it a 3D setting, the liquid flow equation writes:

$$\mathbf{q}_l = -\mathbf{K}\left(\nabla P_l - \rho_l \mathbf{g}\right) - \mathbf{K}_{HT}\nabla T \tag{8}$$

where $\mathbf{K}_{HT}$ is the thermo-osmotic permeability tensor. To illustrate these fluxes a simple test is presented in Figure 3. Figure 3a) shows schematically a heating and hydration experiment in an unsaturated soil. The flow of liquid water driven by the gradient of liquid pressure is governed by Darcy's law and induces a transfer of liquid water from the hydration front inwards (represented by a blue arrow in Figure 3b). The thermo-osmotic flow is controlled by the gradient of temperature and in this test the liquid water moves in the opposite direction (represented by a red arrow in Figure 3b).

<< Include Figure 3 here>>

4. CASE STUDIES

To study the potential effects of thermo-osmotic flows on the response of unsaturated barriers envisioned for the design of nuclear waste disposal two case studies are analyzed. These two cases were selected because they involve different conditions worth to investigate. The case studies are related to two different unsaturated geomaterials (i.e. Case 1 corresponds to a natural rock barrier material, and Case 2 to a manufactured compacted clay barrier); two different heating conditions (i.e. Case 1 involves power control, and Case 2 temperature control); and two different environments (i.e. Case 1 simulates geological repository conditions, and Case 2 model an infiltration cell under controlled conditions in the laboratory).

4.1 Effect of thermo-osmotic flow under repository conditions

The synthetic case proposed by Pollock[18] to study the behavior of a repository for HLW in an unsaturated rock was selected as Case 1 to study the potential effect of thermo-osmotic flows in a simple model of a natural unsaturated barrier aimed at mimicking real repository conditions. Two numerical simulations were performed, one with the standard formulation (i.e. without the osmotic flow) and the other one incorporating the thermo-osmotic phenomenon.

The term representing the thermo-osmotic flow in Eq. (8) was introduced in the general water multi-phase flow model described in Gatmiri and Arson[17] and implemented in the associated Theta-Stock Finite Element program (Arson and Gatmiri[12]). The resulting water flow model accounts for conductive transfer, capillary effects, vaporization and thermo-osmosis. The concept is illustrated on the simplest thermo-osmotic flow scenario possible: the thermo-osmotic conductivity $\mathbf{K}_{HT}$ in Equation 1 is assumed to be a scalar (K_{HT}). This assumption indicates that the thermo-osmotic model does not depend on degree of saturation, neither on dry density (or any other factor), implying that thermo-osmosis has more influence when degree of saturation and/or porosity decrease, because of the associated reduction of the permeability tensor. The basic model proposed here can be upgraded when more experimental information becomes available. There are obviously more phenomena coming into play if chemical reactions are expected to occur.

4.1.1 Geometry, mesh, initial and boundary conditions

The geometry is the one described in Pollock's study of fractured tuff (Pollock[18]). The mesh is a pseudo 1D-column that is 20 meters wide and 475 meters high. The waste is assumed to be stored at a depth of 100 meters. The ground water is located at 500 meters depth. The initial saturation degree of the host rock is around 0.15 and the initial rock void ratio is equal to 0.54. The tunnel is assumed to be long enough to allow a plane strain analysis. An initial

312 geothermal temperature gradient is imposed in the rock mass, the initial surface temperature
313 amounting to 20°C. Fluid pore pressures and suction are initially computed by assuming that
314 the rock mass is in a hydrostatic state. During the simulations, temperatures and pore
315 pressures are maintained to their initial values at the upper and lower boundaries of the
316 model. Nuclear waste is modeled by two elements, which are considered as heating sources.
317 Heat flows are imposed on both of the element horizontal boundaries. The heating power
318 initially amounts to $5 W.m^{-2}$, and then decreases exponentially, as described in Table 1.

319 << Include Table 1 here>>

320 **4.1.2 Constitutive laws**

321 Following the study by Pollock[18], a non-deformable porous medium was considered. The
322 conductivities involved in the flow equations presented in Sections 3.2 depend on the volume
323 fractions of the various constituents present in the rock, mainly: the solid skeleton, liquid
324 water, vapor and gaseous air. The formulas used to obtain the averaged properties of the
325 representative elementary volume from the conductivities of each constituent are provided
326 below, and the corresponding model parameters used for the simulations are given in Table 1.

327 *Hydraulic conductivity to liquid water:*

$$\mathbf{K}_l = k_{l0}\left(S_l\right)^3 \delta \tag{9}$$

328 *Conductivity to gaseous air:*

$$\mathbf{K}_g = \frac{\gamma_g c_g}{\mu_g}\left[e\left(1-S_l\right)\right]^2 \delta \tag{10}$$

329 *Water retention curve:*

$$S_l = \left[1+\left(\frac{s}{P_0}\right)^{\frac{1}{1-\lambda_0}}\right]^{-\lambda_0} \tag{11}$$

330 *Thermal conductivity:*

$$\lambda_T = (1-\varphi_w-\varphi_g)\lambda_s + (\varphi_w+\varphi_g)S_w\lambda_w + (\varphi_w+\varphi_g)(1-S_w)\lambda_{vap} \quad (12)$$

where $\boldsymbol{\delta}$ stands for the second-order identity tensor, k_{l0} is the hydraulic conductivity of the liquid phase in the initial state, γ_g and μ_g are respectively gas specific weight and air dynamic viscosity, e is the current void ratio (constantly equal to the initial void ratio in the present simulations), c_g is a fitting parameter, and λ_s, λ_w and λ_{vap} are the thermal conductivities of the solid skeleton, liquid water and vapor, respectively. In addition, a simplified van Genuchten model (1980) is used for the retention curve (Eq. 10), where P_o is the air entry value and λ a model parameter.

<< Include Table 2 here>>

4.1.3 Model results

The response of the unsaturated tuff rock is studied over 1000 years. Up to 200 years of heating, the evolution of the degree of saturation predicted by the thermo-osmotic model follows the same trends as the one predicted by the classical multi-phase flow model (Fig. 4a and 4b). However the magnitudes are different around the heating source, particularly between 80 meters and 140 meters deep. With the model accounting for thermo-osmotic effects, the saturation degree is approximately twice smaller in this zone than the saturation degree obtained with the reference behavior model. This means that thermo-osmosis originates drying. This is in agreement with the theoretical thermo-osmotic model (Equation 8), stating that fluid flows along decreasing gradients of temperature. Temperature is higher at the vicinity of the heating source, which explains why thermo-osmotic effects tend to reinforce drying near the source. On a closer inspection to these results shown that after 10 years, the rock mass has already been exposed to the highest level of heat power (see Table 1). For both models adopted in this study (with no account of thermo-osmosis in Fig.4.a and with thermo-osmosis in Fig.4.b), we observe a desaturation 20 meters both above and below

354 the heat source: this drying effect is due to vaporization, which is enhanced by thermo-
355 osmosis in Fig.4.b. Drying by vaporization and/or thermo-osmosis induces a flow of water
356 towards the top and bottom boundaries of the domain. The heat source is located at a distance
357 of 100 meters from the top boundary and at a distance of 400 meters from the bottom
358 boundary, which are both drained (fixed pore pressures). Over time (plots corresponding to
359 500 and 1000 years), water flows out by the top boundary. By contrast, the water front does
360 not reach the bottom boundary so that upon cooling (i.e. for time>500 years, see Fig.5), so
361 that water vapor condensates and flows back to the heat source by capillarity. Non-symmetric
362 boundary conditions explain why, in the long term and outside of the influence zone for
363 depths in the interval [80m, 120m], it is observed a desaturation above the heat source and a
364 re-saturation below the heat source.
365 Temperature reaches a peak at the depth of the source, and decreases as the distance to the
366 source increases. The zone of influence of the thermo-osmotic flow is more obvious in Figure
367 4 which illustrates the impact of water flow on the degree of saturation. The effect on
368 temperature is indirect: the account for thermo-osmosis changes the values taken by the
369 degree of saturation, hence the volume fractions of liquid and gas, which weigh the average
370 thermal conductivity of the rock mass. From Figure 5, it can be seen that temperature
371 predictions differ only between 50 and 200 years of exposure, between 90 meters deep and
372 110 meters deep (i.e. +/- 10 meters away from the heat source). The maximum difference of
373 temperature observed in the simulations is about 10°C.
374 << Include Figure 4 here>>
375 If thermo-osmosis is accounted for (Figure 5.b), temperature remains elevated around the
376 nuclear waste for a longer period than if thermo-osmosis is not accounted for (Figure 5.a).
377 This could be expected, since with the values of thermal conductivities used in these
378 simulations (Table 2), the thermal conductivity of the unsaturated rock (given by Eq. (12))

379 should decrease as the degree of saturation decreases. Thermo-osmotic drying effects noticed
380 in Figure 4 are thus expected to reduce the thermal conductivity of the rock around the
381 nuclear waste disposal, which explains why the temperature decrease normally expected as
382 the heat power decreases is delayed when thermo-osmosis is accounted for in the model. As a
383 conclusion, the effect of thermo-osmotic flow can be significant in problems related to
384 nuclear waste disposals, which involve long-term coupled flow processes.

385 << Include Figure 5 here>>

386 **4.2 Effect of thermo-osmotic flow in a clayey engineered barrier material**

387 Case 2 corresponds to the modeling of two infiltration tests carried out to gain a better
388 understanding of the thermal effect on the hydration of clayey barrier materials.
389 The infiltration tests were performed by CIEMAT (Spain) in cylindrical cells 40 cm long and
390 7 cm diameter. They were made of Teflon© to minimize lateral heat conduction, and were
391 externally covered with steel semi-cylindrical pieces to prevent the deformation of the cell by
392 bentonite swelling. In one of the tests (i.e., GT40) the clay was heated through the bottom
393 surface at a constant temperature of 100ºC. The other test (i.e., IT40) was carried out at
394 isothermal conditions. The cells were instrumented with relative humidity and temperature
395 sensors placed inside the clay at three different levels separated by 10 cm. The relative
396 humidity and temperature evolution at different levels inside the clay were recorded. The
397 FEBEX clay was compacted with its hygroscopic water content (around 14 %) at an initial
398 nominal dry density of 1.67 Mg/m^3. Granitic water was injected through the upper part of the
399 cells (in both tests) at a pressure of 1.2 MPa. Figure 6a) shows a photo of the cells during
400 operation, while Figure 6b) illustrates the experimental setup showing its main components.
401 More details can be found in Villar and Gómez-Espina[30].

402 << Include Figure 6 here>>

403 A very slow hydration was observed in the test under thermal gradient (i.e. GT40). To
404 explain the delay in the hydration three different possible phenomena were investigated: i)
405 presence of a threshold gradient in the flow law; ii) evolution of clay micro-fabric during
406 hydration; and iii) effect of thermo-osmotic flows.
407 The threshold gradient phenomenon considers a lower limit of applicability of the Darcy's
408 law. Some experimental evidences show that under low hydraulic gradients, Darcy's simple
409 relationship does not rule the liquid flow in some geomaterials, especially in soils containing
410 active clay minerals. The strong clay-water interactions typically observed in this type of
411 soils is suggested to explain this non-Darcian flow behavior (e.g. Bear[19]). Phenomenon ii) is
412 associated with the dynamic character of the clay fabric during wetting. The fabric of
413 compacted clays consist of dense aggregates of clay particles with intra-aggregate pores
414 (micropores) between them. The arrangement of these clay aggregates conforms a granular
415 skeleton of the material with inter-aggregate spaces (macropores). When a clay barrier is
416 hydrated, the clay aggregates tend to adsorb water and swell. Under constant volume
417 conditions (as the ones prevailing in HLW repositories because of the high confinement) the
418 expansion of the microstructure is made possible by the reduction of the macropores, which
419 in turns significantly influence clay permeability and hence barrier hydration kinetic. This
420 paper focuses on the analysis related to phenomenon iii), explained in detail in the following
421 sections. More information about the different analyses can be found in Aponte[31]. The
422 modeling of this cells incorporating the evolution of the micro-fabric is discussed in Sanchez
423 et al.[32].
424 The GT40 and IT40 tests were modeled using two THM approaches, as follows: i) a standard
425 THM formulation that does not include thermos-osmotic effects (i.e. Olivella et al.[27],
426 introduced in Section 3.1 to 3.3), and ii) an improved formulation incorporating thermos-
427 osmotic flows (as indicated in Section 3.4).

As for the analysis i), the model known as Operational Base Case (OBC) was adopted in this study. The OBC model was used in a number of simulations related to others FEBEX experiments and it can be considered as a 'standard' approach to analyze this type of problem. The OBC has been used extensively (e.g. Villar et al.[4], Gens et al.[33], Sánchez et al.[17,34]). As for the analysis ii), a thermo-osmotic flow model (coded as THO hereafter) was incorporated in the THM formulation proposed by Olivella et al.[27]). The modified flow model of Eq. (8) was implemented in the finite element program CODE_BRIGHT (Olivella et al.[13]) and used for the numerical analysis. CODE_BRIGHT has been widely validated and satisfactorily applied in a variety of coupled THM problems involving expansive clays (e.g. Åkesson et al.[35], Gens et al.[33]). In the following sections the main components of the model, the constitutive laws and the main results are discussed.

4.2.1 Geometry, mesh, initial and boundary conditions

A 1-D axis-symmetrical model was adopted in the analyses. A mesh of one hundred (100) elements was prepared. A sensitivity analysis was carried out to verify that the model results do not depend on the mesh. The initial and boundary conditions of the model were imposed in order to be the closest possible to the experiments. The initial water content of the bentonite block is close to 14%, from the retention curve adopted an initial value of suction close to 140 MPa was assumed. An initially uniform temperature of 22 °C was assumed. An initial hydrostatic stresses of 0.15 MPa was adopted.

As for the boundary conditions of the GT40 cell, a temperature of 100 °C was imposed at the contact between heater and bentonite (i.e. the bottom of the cell), while a constant water pressure of 1.2 MPa was imposed at the other extreme of the cell (i.e. upper part). The thermal boundary condition along the sample was adopted in order to adjust the temperature field, in that sense a temperature of 23 °C was fixed with a radiation coefficient of 1 (one). Finally, a constant gas pressure (0.1 MPa) was adopted in the analyses. For the IT40 cell,

453 similar boundaries conditions were adopted for the mechanical and hydraulic problems, but
454 isothermal conditions were considered.

455 **4.2.2 Constitutive laws**

456 In this section the constitutive equations that complement the ones presented in Section 3.2
457 are briefly introduced. The laws and parameters adopted for the two numerical models (i.e.
458 OBC and THO) are identical, but for the incorporation of the thermos-osmotic law in the
459 THO model.

460 *Hydraulic models*

461 The permeability tensor for the liquid flow presented in Eq. (5) $\mathbf{K}_l$ is evaluated according to:

$$\mathbf{K}_\alpha = \mathbf{k}\frac{k_{r\alpha}}{\mu_\alpha}; \qquad \alpha = l, g \tag{2}$$

462 where $\mathbf{k}$ is the intrinsic permeability tensor, μ_l is the liquid dynamic viscosity and k_{rl} is the
463 liquid relative permeability. The dependence of intrinsic permeability on porosity was based
464 on Kozeny's law:

$$\mathbf{k} = k_0 \frac{n^3}{(1-n)^2}\frac{(1-n_0)^2}{n_0^3}\mathbf{I} \tag{14}$$

465 where k_0 is the reference saturated permeability at the reference porosity n_0. Permeability
466 tests performed on saturated samples have been used to adopt the reference values: k_0 =
467 $1.9\text{x}10^{-21}$ m^2 for a porosity of 0.40 (Figure 7.a). The well-known power law has been adopted
468 to describe the dependence of liquid permeability on degree of saturation:

$$k_{rl} = S_l^{n_s} \tag{15}$$

469 A value of n_s = 3 was determined from back-calculating hydration tests on FEBEX bentonite
470 (Huertas et al.[36]).

471 As for the water retention curve, the van Genuchten[37] model presented in Eq. (11) was
472 modified for the bentonite, as follows:

$$S_l = \left[1+\left(\frac{s}{P_o}\right)^{\frac{1}{1-\lambda_o}}\right]^{-\lambda_o} f_d \quad \text{a)}; \qquad f_d = \left(1-\frac{s}{P_d}\right)^{\lambda_d} \quad \text{b)} \tag{16}$$

where the function f_d is included in order to model properly the high suction range. P_d is related to the suction at 0 degree of saturation and λ_d is a model parameter. When $\lambda_d = 0$ Eq. (12) is recovered. Figure 7.b) presents the results of tests carried out at conditions of constant volume on FEBEX bentonite (Huertas et al., 2006), alongside the adopted model is presented. Model parameters are: $P_0 = 20$ MPa; $\lambda_0 = 0.18$, $P_d = 1100$ MPa, and $\lambda_d = 1.10$.

Note that experimental data is lacking for the coefficient associated with the thermo-osmotic flow (K_{HT}) in FEBEX bentonite. .. Based on published data for other clayey materials (i.e., Djeran[23]and Soler[24]), the thermo-osmotic constant adopted in the numerical analysis was 5.60 x 10^{-12} m^2/K/s.

Thermal model

The thermal conductivity adopted for the Fourier's law (Eq. 7) depends on the saturation of the clay and is expressed by the geometric mean of the thermal conductivities of the components:

$$\lambda = \lambda_{sat}^{S_l} \lambda_{dry}^{(1-S_l)} \tag{17}$$

Based on experimental results (Figure 7.c), the following thermal conductivities were adopted: λ_{dry}=0.47 and λ_{sat}=1.15.

<< Include Figure 7 here>>

Mechanical model

The Barcelona Basic Model (BBM) was adopted to model the mechanical behavior of the FEBEX clayey barriers (i.e. Gens et al.[33]and Sanchez et al.[17]). The BBM is an elasto-plastic strain hardening model, which extends the concept of critical state for saturated soils to the unsaturated conditions and it is able to reproduce many of the basic patterns of behavior

observed in unsaturated soils (Alonso et al.[38]). The BBM considers two independent stress variables: the net stress ($\boldsymbol{\sigma}$), computed as the excess of the total stresses over the gas pressure ($\boldsymbol{\sigma}_t$-$\mathbf{I}p_g$), and the matric suction (s), computed as the difference between gas pressure and liquid pressure. The model is formulated in terms of the three stress invariants (p; J; θ) ; suction and temperature. In the BBM the yield surface depends also on the matric suction. The trace of the yield function in the isotropic p-s plane is called the *LC* (Loading-Collapse) yield curve, because it represents the locus of activation of irreversible deformations due to loading increments or wetting (collapse compression). The position of the *LC* curve is given by the value of the hardening variable p_o^*, which is the apparent pre-consolidation yield stress of the saturated state. The BBM was extended to non-isothermal condition following the approach suggested by Gens[39]. It was considered that thermal changes affect both elastic and plastic behaviors. Pre-consolidation pressure is affected by temperature assuming that temperature increases reduce the size of the yield surface and the strength of the material. The BBM yield surface (F_{LC}) is then expressed as:

$$F_{LC} = 3J^2 - \left[\frac{g(\theta)}{g(-30^\circ)}\right]^2 M^2 (p + p_s)(p_0 - p) = 0 \tag{18}$$

where M is the slope of the critical state, p_o is the apparent unsaturated isotropic pre-consolidation pressure at a specific value of suction, and p_s considers the dependence of shear strength on suction and temperature. When yielding takes place the increment of plastic deformations is evaluated through:

$$\dot{\boldsymbol{\varepsilon}}^p_{LC} = \lambda_{LC} \frac{\partial G}{\partial \boldsymbol{\sigma}} \tag{19}$$

where λ_{LC} is the plastic multiplier and G is the plastic potential (defined in the Appendix).

The hardening law is expressed as a rate relation between the volumetric plastic strain and the saturated isotropic pre-consolidation stress 'p^*_0', according to:

$$\frac{\dot{p}_0^*}{p_0^*} = \frac{(1+e)}{(\lambda_{(0)} - \kappa)} \dot{\varepsilon}_v^p \tag{20}$$

where e is the void ratio, ε_v^p is the volumetric plastic strain, κ is the elastic compression index for changes in p, and $\lambda_{(0)}$ is the stiffness parameter for changes in p for virgin states of the soil in saturated condition.

Because of the high compaction to which the bentonite blocks were subjected to, the description of the behavior of the material inside the yield surface is particularly important. According to the adopted parameters (Table 3), it is expected that the whole stress path will lie inside the BBM yield surface. The variation of stress-stiffness with suction and the variation of swelling potential with stress and suction were considered. The resulting elastic model is the following:

$$\dot{\varepsilon}_v^e = \frac{\kappa}{(1+e)} \frac{\dot{p}}{p} + \frac{\kappa_s}{(1+e)} \frac{\dot{s}}{(s+0.1)} + (\alpha_0 + \alpha_2 \Delta T)\dot{T} \quad \text{a)}; \qquad \dot{\varepsilon}_s^e = \frac{\dot{J}}{G_t} \quad \text{b)} \tag{21}$$

where κ_s is the macrostructural elastic stiffness parameter for changes in suction, G_t is the shear modulus; α_0 and α_2 are model parameters related to temperature. κ, κ_s and G_t are evaluated according to:

$$\kappa = \kappa_i (1 + \alpha_s s) \quad \text{a)}; \qquad \kappa_s = \kappa_{s0} \left(1 + \alpha_{sp} \ln p / p_{ref}\right) \text{b)}; \qquad G_t = \frac{3(1-2\mu)K}{2(1+\mu)} \quad \text{c)} \tag{22}$$

where μ is the Poisson's coefficient; α_s and α_{sp} are model parameters; and the bulk modulus (K) is obtained from (A5), see Appendix. They were determined from the experimental laboratory campaign carried out during the FEBEX project (Huertas et al.[36]). As an example, Figure 7.d) shows the results of two swelling pressure tests: SP1 and SP2 (Lloret et al.[3]), used for the experimental calibration of the model, together with the stress path computed with the model.

533 The main parameters of the OBC model are listed in Table 3

534 << Include Table 3 here>>

535 **4.2.3 Model results**

536 Figure 8 presents the results in terms of relative humidity for the cell IT40. Figures 9 and 10
537 show the time evolution of temperature and relative humidity in cell GT40, respectively.. In
538 these three plots the experimental data is represented with symbols, the OBC results with
539 dash lines, and the THO outputs with solid lines. All the results are presented for a period of
540 10 years.

541 As for the relative humidity results in the IT40 cell, it can be seen that the OBC model predict
542 a relatively quick saturation of the clay, faster than the observed experimental behavior. In
543 the IT40 cell, since no gradient of temperature is imposed, the results obtained with the THO
544 model are similar to those obtained with the OBC model..

545 In relation to the evolution of temperature in the cell GT40, both models reproduce quite well
546 the thermal field. The OBC model tends to predict higher temperatures, particularly at
547 advanced stages of the test. This is because the higher saturation predicted by the OBC model
548 (which can be inferred from Figure 10) results in higher thermal conductivities and therefore
549 higher temperatures globally.

550 As for the evolution of relative humidity in the cell GT40, it can be seen that the OBC model
551 predicts a quite fast hydration. Particularly in zones near the heater, the difference between
552 experimental observations and model are quite noticeable. A similar trend was detected in the
553 'mock-up test', which is a large clay-barrier heating test that is being carried out at CIEMAT
554 facilities in the context of the FEBEX project (e.g. Sánchez et al.[17]). According to the OBC
555 model, the cell GT40 is practically fully saturated after 10 years of heating and hydration,
556 while the experimental observations indicate that an important portion of the cell remains
557 quite dry after this period of time. It is observed that near the heater there is a significant

558 drying of the clay. The OBC model under estimates this drying. The OBC model predicts a
559 moderate drying at the beginning of the experiment, up to around 200 days, afterwards the
560 advective flux of liquid water driven by the gradient of liquid pressure (i.e., Darcy's flow)
561 dominates fluid transport and the water coming from the top of the cell starts to hydrate the
562 bentonite progressively.
563 In the THO model there are two main phenomena associated with the movement of liquid
564 flow. The direct process, related to the Darcy's law, which tends to move water from the
565 hydration front (i.e., top of the cell) to the heater, where the lower liquid pressures prevail
566 (i.e., bottom of the cell). However, the thermo-osmotic flow tends to transfer liquid water
567 from the heater zone to the hydration front (i.e., from higher to lower temperatures). These
568 coupled processes trigger a flux of water opposite to the Darcy's one, inducing an additional
569 drying of the clay near the heater. According to the model, these two opposite fluxes cancel
570 out (practically) at advanced stages of hydration preventing the zones near the heater to
571 hydrate. As a result, the model incorporating thermo-osmotic flows is able to explain the
572 experimental observations.

573 **4.2.4 Discussion**

574 The experimental results and model show that the barrier remained unsaturated for a very
575 long time. It is unlikely that this will happen in actual repositories, because in the experiment
576 the temperature was kept constant at the contact between heater and bentonite (and equal to
577 100 ºC), but, under real repository conditions, the waste temperature reduces progressively
578 over time (e.g., Table 1) and therefore the effect of the thermo-osmotic flow will vanish
579 progressively.
580 The other two phenomena considered to study the low hydration of the barrier (i.e. the
581 presence of a threshold gradient in the flow law, and micro-fabric evolution) were also able to
582 reproduce quite satisfactorily the hydration delay i observed in the hot zones (Aponte[29]). The

583 effect of a threshold gradient in the flow law was implemented by introducing a nonlinear
584 relationship between the flux and the hydraulic gradient in the Darcy law for low hydraulic
585 gradients. The effect of the micro fabric was incorporated via an elasto-plastic double
586 structure model. This case is analyzed in detail in Sanchez et al.[30].
587 Because of the scarcity of experimental data available to formulate these 'non-standard flow
588 models' the results have mainly a qualitative value. However, these are all plausible flow
589 phenomena in porous media and it is relevant to see that they were able to provide an
590 explanation to the kinetic of hydration observed in the experiments. After all, each of these
591 flow phenomena does not exclude the others and it is possible that an explanation for the
592 whole behavior of the barrier would require the combinations of several of them. The long-
593 term behavior of this ongoing experiments and the planned post-mortem study will also help
594 elucidating the actual state of the barrier material and to understand better its behavior.

595 **5. CONCLUSION**

596 Waste storage structures have to be reliable over hundreds of years. Simultaneous heating and
597 hydration in a porous medium triggers a number of direct and coupled thermo-hydro-
598 mechanical processes. Common mathematical formulations consider direct processes only.
599 However coupled processes may be also relevant for the design of nuclear waste disposals.
600 By contrast with models of direct flow phenomena, thermo-osmotic models can explain the
601 delayed hydration of the engineering barrier around nuclear waste disposals. The simulation
602 results obtained on a large-scale heating test show that thermo-osmotic flow may play an
603 important role in the long-term hydration state of the geological barrier used for nuclear
604 waste disposals. The presence of thermo-osmotic flows could also explain the apparent low
605 hydration observed in a heating and hydration lab test aimed at mimicking the behavior of
606 clayey barrier materials under actual hydraulic and thermal gradients. It was shown that the

607 model incorporating thermo-osmotic flow was able to reproduce quite satisfactorily the main
608 patterns of behavior observed in the experiments.
609 Similar effects (with very likely significant consequences) can be anticipated in other
610 problems involving thermal gradients. For example, in geothermal applications, thermo-
611 osmotic flow may have an influential role in the heat transfer process (for example, by
612 inducing higher temperatures in the rock mass around the borehole, like in the first case
613 study). This may affect the efficiency and profitability of the whole geothermal system.
614 Unfortunately the limited experimental information associated with thermo-osmotic
615 coefficients has prevented any reliable quantification of this phenomenon in practical
616 applications.
617

618 **REFERENCES:**

619 [1] Pusch R. Swelling pressure of highly compacted bentonite. *Technical Report, SKBF*
620 *KBF* 1980;90-13.

621 [2] Delage P, Cui YJ, Tang AM. Clays in radioactive waste disposal. J. *of Rock Mech.*
622 *Geotech. Engg*. 2010;2(2):111-123.

623 [3] Lloret A, Villar MV, Sánchez M, Gens A, Pintado X, Alonso EE. Mechanical ,behaviour
624 of heavily compacted bentonite under high suction changes. *Géotechnique* 2003;53(1):
625 27-40.

626 [4] Villar MV, Sánchez M, Gens A. Behaviour of a bentonite barrier in the laboratory:
627 Experimental results up to 8 years and numerical simulation. *Physics and Chemistry of*
628 *the Earth* 2008;33:S476–S485.

629 [5] Cleall P.J., Singh R.M. and Thomas H.R. (2013). Vapour transfer in unsaturated
630 compacted bentonite. *Geotechnique*, 63(11):957-964. [doi:10.1680/geot.12.P.147].

631 [6] Cleall P.J., Singh R.M. and Thomas H.R. (2011). Non-isothermal moisture movement
632 in unsaturated kaolin: An experimental and theoretical investigation. *ASTM*
633 *Geotechnical Testing Journal*, 34(5): 514-524. [doi: 10.1520/GTJ1035 85].

634 [7] Gens A, Alonso EE. A framework for the behaviour of unsaturated expansive clays.
635 *Can. Geotech. Jnl*. 1992;29:1013-1032.

636 [8] Cui Y, Sultan N, Delage P. A thermomechanical model for clays. Can. Geotech. Jnl.
637 2000;37:607-620.

638 [9] Hueckel T, Pellegrini R. Reactive plasticity for clays: application to a natural analog of
639 long-term geomechanical effects of nuclear waste disposal. *Engineering Geology*
640 2002;64:195-215.

641 [10] Sánchez M, Gens A, Guimaraes L, Olivella S. A double structure generalized plasticity
642 model for expansive materials. *Int. Jnl. Numer. Anal. Meth. Geomech*. 2005;29:751–
643 787

644 [11] François B, Laloui L. ACMEG ‐ TS: A constitutive model for unsaturated soils under
645 non ‐ isothermal conditions. *International Journal for Numerical and Analytical*
646 *Methods in Geomechanics* 2008;32(16):1955-1988

647 [12] Arson C, Gatmiri B. Thermo-Hydro-Mechanical Modeling of Damage in Unsaturated
648 Porous Media: Theoretical Framework and Numerical Study of the EDZ, *International*
649 *Journal for Numerical and Analytical Methods in Geomechanics*, 2012;36:272-306

650 [13] Olivella S, Gens A, Carrera J, Alonso EE. Numerical formulation for a simulator
651 (CODE-BRIGHT) for the coupled analysis of saline media. *Engineering Computations*
652 1996;13(7):87-112.

653 [14] Rutqvist J, Borgesson L, Chijimatsu M, Nguyen T, Jing L, Noorishad J, Tsang C.
654 Coupled thermo-hydro-mechanical analysis of a heater test in fractured rock and
655 bentonite at Kamaishi mine - comparison of field results to predictions of four finite
656 element codes. *International Journal of Rock Mechanics and Mining Sciences*
657 2001;38:129–142.

658 [15] Gatmiri B, Arson C. Stock, a powerful tool for thermohydromechanical behaviour and
659 damage modelling of unsaturated porous media. *Computers and Geotechnics*
660 2008;35(6):890-915

661 [16] Thomas H, Cleall P, Chandler N, Dixon D, Mitchell H. Water infiltration into a large-
662 scale in-situ experiment in an underground research laboratory. *Géotechnique*
663 2003;53(2):207-224.

664 [17] Sánchez M, Gens A, Olivella S. THM Analysis of a large scale heating test
665 incorporating material fabric changes. *Int. Jnl. Numer. Anal. Meth. Geomech*
666 2012;36(4):391-421.

667 [18] Pollock DW. Simulation of fluid flow and energy transport processes associated with
668 high-level radioactive waste disposal in unsaturated alluvium. *Water Resources*
669 *Research* 1986;22(5):765-775

670 [19] Bear J. Dynamics of fluids in porous media. 1972 Dover Edit.

671 [20] Lippmann G. Endosmose entre deux liquides de meme compostion chimique et de
672 temperature differentes. *Comptes Rendus Hebdomadaires*, 1907;145:104-105.

673 [21] Srivastava RC, Avasthi PK. Non-equilibrium kaolinite. *Jnl. Hydrol*. 1975;24:111–120

674 [22] Horseman ST, McEwen TJ. Thermal constraints on heat emitting waste in argillaccous
675 rocks. *Engineering Geology* 1996;41:5-16

676 [23] Djeran I. Étude des duffusions thermique et hydraulique dans una argile soumise áun
677 champ de température. *Sciences et techniques nucléaires rapport*. Commission des
678 Communautés européennes, 1993;ISBN 1018-5593.

679 [24] Soler J. The effect of coupled transport phenomena in the Opalinus Clay and
680 implications for radionuclide transport. *Journal of Contaminant Hydrology* 2001;53:63-
681 84.

682 [25] Bing Bai. Thermal consolidation of layered porous half space to variable thermal
683 loading. *Applied Mathematics and Mechanics* (English Edition), 2006;27(11):1531–
684 1539

685 [26] Chen Y. Zhou Ch. Jing L. Modeling coupled THM processes of geological porous
686 media with multiphase flow: Theory and validation against laboratory and field scale
687 experiments. *Computers and Geotechnics* 2009;36(8):1308–1329.

688 [27] Olivella S, Carrera J, Gens A, Alonso EE. Non-isothermal multiphase flow of brine and
689 gas through saline media. *Transport in porous media* 1994;15:271-293.

690 [28] Philip J,. de Vries DA. Moisture movement in porous materials under temperature
691 gradients. *Transactions, American Geophysical Union* 1957;38(2):222-232

692 [29] Milly PC. Moisture and heat transport in hysteretic, inhomogeneous porous media: a
693 matric head-based formulation and a numerical model. *Water Resour. Res*.
694 1982;18(3):489–498.

695 [30] Villar MV, Gómez-Espina R. Report on thermo-hydro-mechanical laboratory tests
696 performed by CIEMAT on FEBEX bentonite 2004-2008. 2009; CIEMAT, Madrid

697 [31] Aponte F. Thermo-Hydro-Mechanical coupled analysis in low permeability media
698 under nuclear waste repository conditions. *MSc Thesis, Texas A&M University*;
699 2013:217

700 [32] Sánchez M, Gens A, Villar MV, Olivella S. A Fully Coupled THM Double Porosity
701 Formulation for Unsaturated Soils. *International Journal of Geomechanics* 2016
702 (acepted).

703 [33] Gens A, Sanchez M, Guimaraes L, Alonso EE, Lloret A, Olivella S, Villar MY, Huertas
704 F..A full scale in situ heating test for high level nuclear waste disposal - Observations,
705 analysis and interpretation. *Géotechnique* 2009;59(4): 377–399

706 [34] Sánchez M, Gens A, Guimarães L. Thermal–hydraulic–mechanical (THM) behaviour
707 of a large-scale in situ heating experiment during cooling and dismantling. *Canadian*
708 *Geotechnical Journal* 2012;49(10):1169-1195.

709 [35] Åkesson M, Jacinto A, Gatabin C, Sánchez M, Ledesma A. Bentonite THM behaviour
710 under high temperature gradients. Experimental and numerical analysis. *Géotechnique*;
711 2003;59(4): 307-318.

712 [36] Huertas F, Farina P, Farias J, Garcıa-Sineriz JL, Villar MV, Fernandez AM, Martın PL,
713 Elorza F J, Gens A, Sanchez M, Lloret A, Samper J, Martınez M. Full-scale engineered
714 barrier experiment. *Updated Final Report, Technical Publication 05-0/2006*. 2006;
715 Madrid: Enresa.

716 [37] van Genuchten MTh. A closed-form equation for predicting the hydraulic conductivity
717 of unsaturated soils. *Soil Science Society of America Journal* 1980;44(5):892–898.

718 [38] Alonso EE, Gens A. Josa A. A constitutive model for partially saturated soils.
719 *Géotechnique* 1990;40(3):405-430.

720 [39] Gens A. Constitutive Laws. Modern issues in non-saturated soils. *Springer-Verlag*
721 1995;129-158.

722

723

724
725

APPENDIX

The *BBM* model was adopted to describe the mechanical behavior of the clay. The corresponding yield surface (F_{LC}) is given by (25) and the plastic potential (G) is expressed as:

$$G = \alpha_G 3J^2 - \left[\frac{g(\theta)}{g(-30^o)}\right]^2 M^2 (p + p_s)(p_0 - p) = 0 \quad \text{(A1)}$$

where α_G is determined according to (Alonso et al., 1990) . The dependence of the tensile strength on suction and temperature is given by:

$$p_s = k s_1 e^{-\rho \Delta T} \quad \text{(A2)}$$

where k and ρ are model parameters. The dependence of p_0 on suction is given by:

$$\text{(a) } p_0 = p_c \left(\frac{p_{0T}^*}{p_c}\right)^{\frac{\lambda_{(0)} - \kappa}{\lambda_{(s)} - \kappa}} ; \qquad \text{b) } p_{0T}^* = p_0^* + 2\left(\alpha_1 \Delta T + \alpha_3 \Delta T |\Delta T|\right) \quad \text{(A3)}$$

where p_c is a reference stress, α_1 and α_3 are models parameters. $\lambda_{(s)}$ is the compressibility parameter for changes in net mean stress for virgin states of the soil. This parameter depends on suction according to:

$$\lambda_{(s)} = \lambda_{(0)} \left[r + (1 - r)\exp(-\zeta s_1)\right] \quad \text{(A4)}$$

where r is a parameter which defines the minimum soil compressibility (at infinite suction) and ζ is a parameter which controls the rate of decrease of soil compressibility with suction. The bulk modulus (K) for changes in mean stress is evaluated with the following law:

$$K = \frac{(1 + e)}{\kappa} p \quad \text{(A5)}$$

where κ is evaluated according to.

$$\kappa = \kappa_i (1 + \alpha_s s_1) \quad \text{(A6)}$$

The macrostructural bulk modulus for changes in suction is computed considering the following law:

$$K_s = \frac{(1 + e)(s + p_{atm})}{\kappa_s} \quad \text{(A7)}$$

where κ_s is evaluated according to.

$$\kappa_s = \kappa_{s0}\left(1+\alpha_{sp}\ln p/p_{ref}\right) \tag{A8}$$

The bulk modulus for changes in temperature is computed considering the following law:

$$K_T = \frac{1}{\left(\alpha_0+\alpha_2\Delta T\right)} \tag{A9}$$

where α_o and α_2 are parameters related to the elastic thermal strain.

Figure

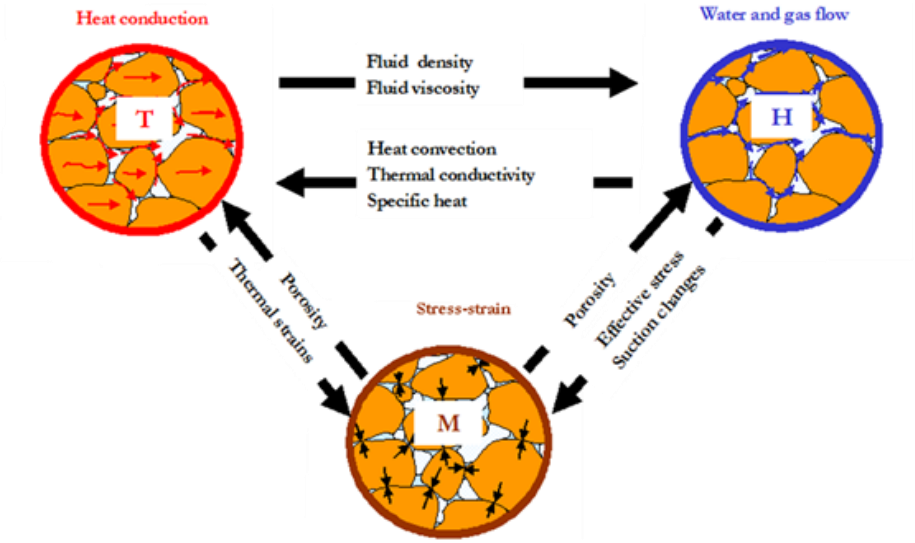

Figure 1. Main THM phenomena in porous media and their mutual interactions.

Flow	Gradients		
	Hydraulic Head	Chemical Concentration	Temperature
Fluid	Darcy's Law (Hydraulic Conduction)	Chemical Osmosis	Thermo Osmosis
Solutes	Ultra Filtration	Fick's Law (Diffusion)	Soret Effect (Thermal Diffusion)
Heat	Thermo Filtration (Isothermal Heat Transfer)	Dufour Effect	Fourier's Law (Thermal Conduction)

Figure 2. Direct and coupled flow processes

a)

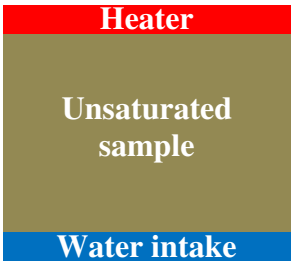

b)

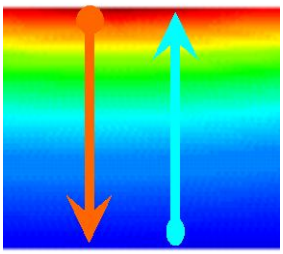

$$\mathbf{q}_l = -\mathbf{K}_{HT}\nabla T - \mathbf{K}\left(\nabla P_l - \rho_l \mathbf{g}\right)$$

Figure 3. Schematic representation of a heating and hydration test of an unsaturated sample: a) schematic represation of the test, b) anticipated Darcy's and thermos-osmotic flows.

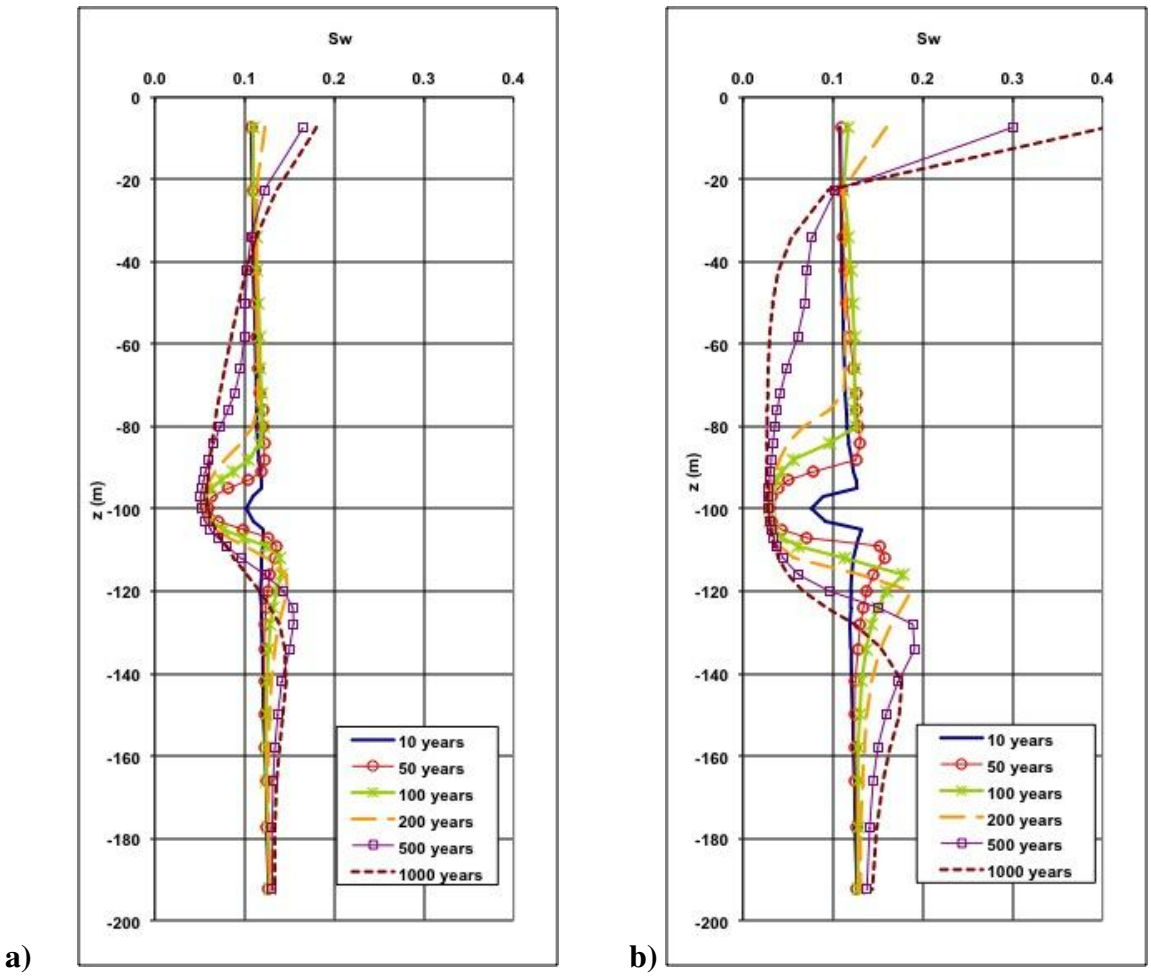

Figure 4: Liquid saturation degree simulated in a heated unsaturated tuff rock mass: a. reference model (without thermo-osmosis); b. modified model incorporeating thermo-osmosis.

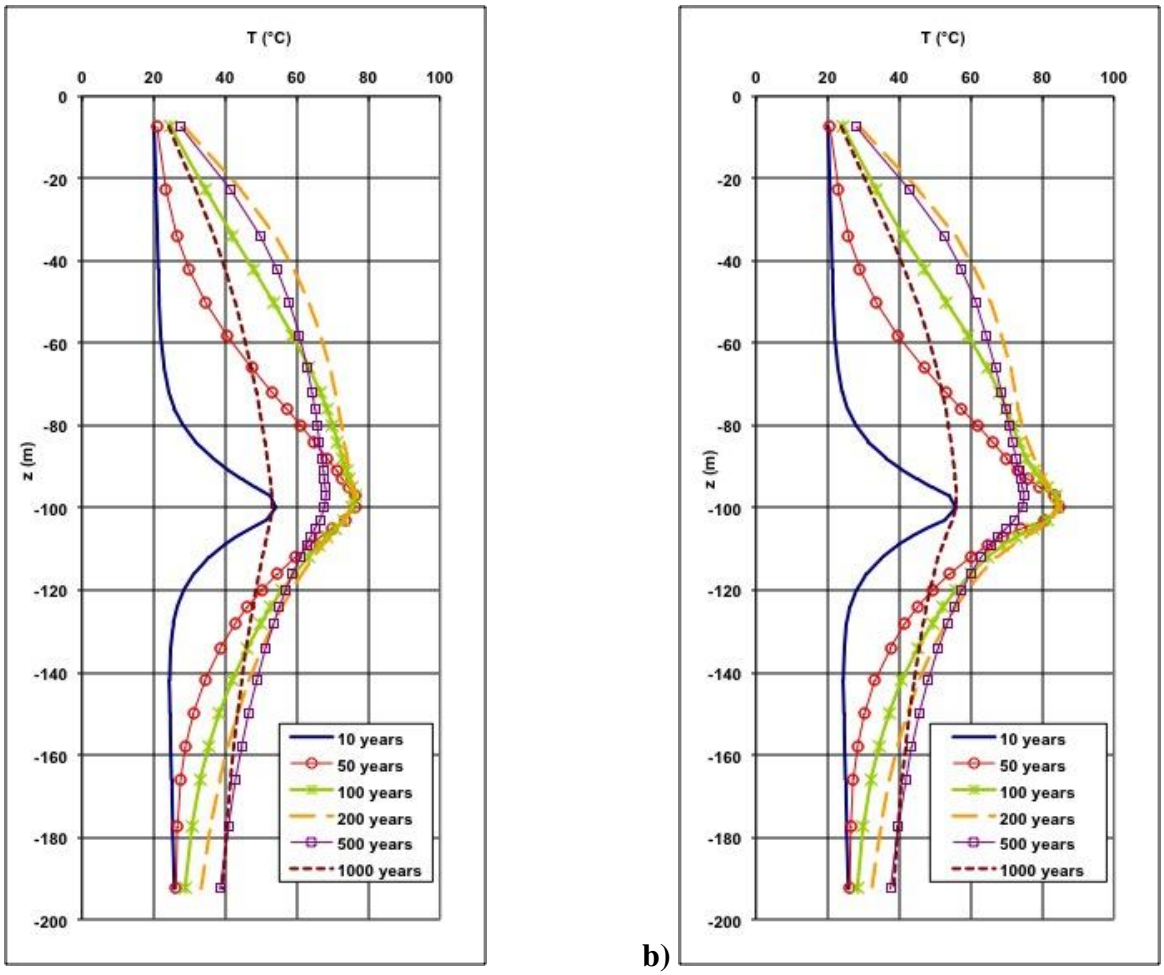

Figure 5. Temeprature simulated in a heated unsaturated tuff rock mass: a. reference model (without thermo-osmosis); b. modified model incoirporating thermo-osmosis.

a)

b)

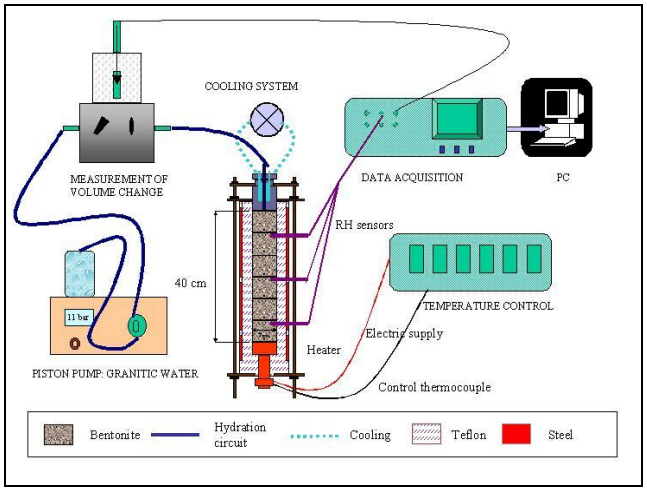

Figure 6. Infiltration cells: a) photo during operation, isothermal, I40 (left) and thermal gradient, GT40 (right); and b) experimental setup showing the main components (Villar and Gómez-Espina[30]).

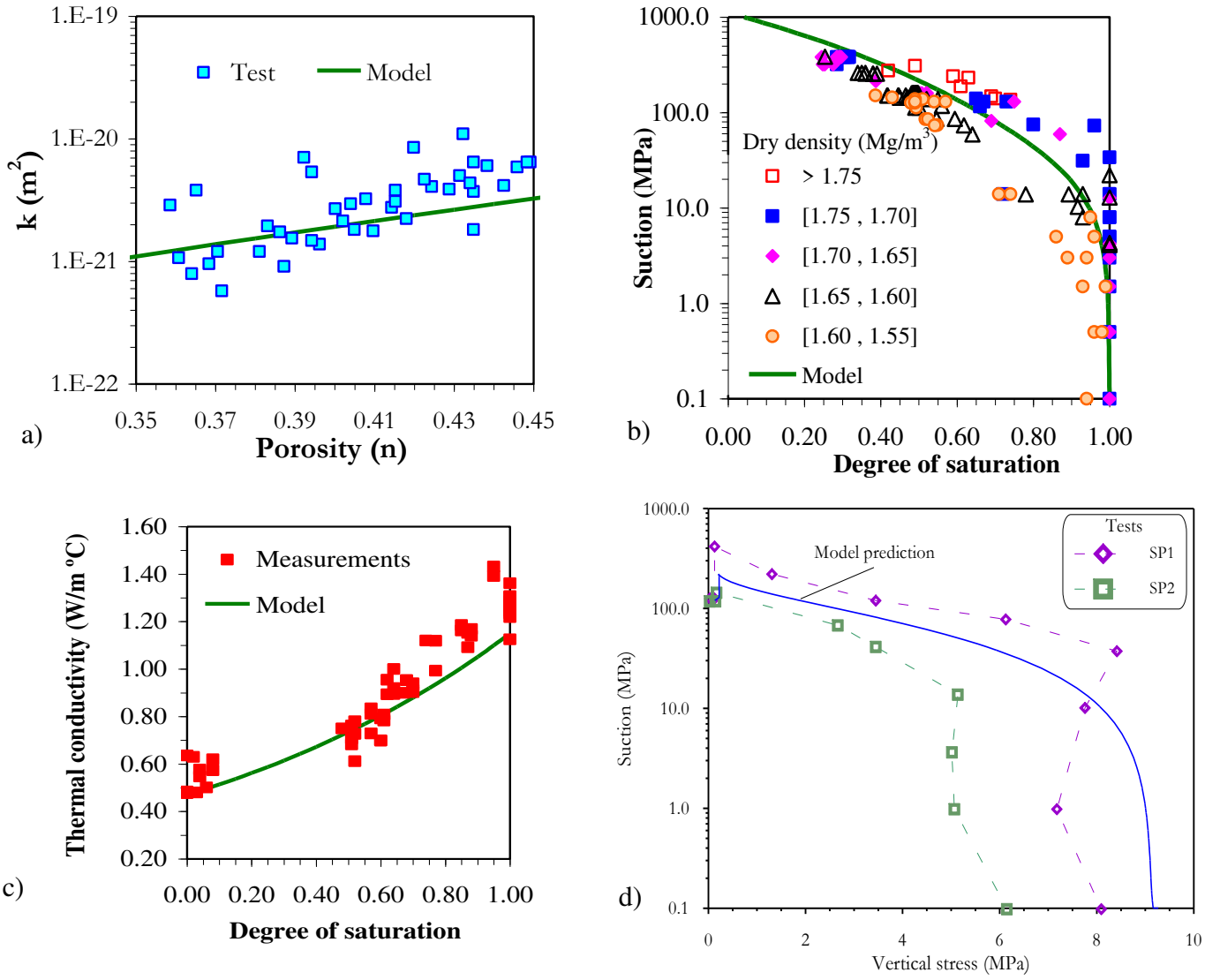

Figure 7. Main constitutive laws. a) Mechanical: computed stress path for swelling pressure tests using the BBM. Experimental results (SP1 and SP2 paths) are provided for comparison. b) Hydraulic: variation of saturated permeability with porosity. Experimental data and adopted model for the intrinsic permeability law. c) Hydraulic: retention curve adopted in the analyses, together with the experimental data for FEBEX bentonite (symbols). d) Thermal: Thermal conductivity: FEBEX bentonite experimental results (symbols) and model fitting.

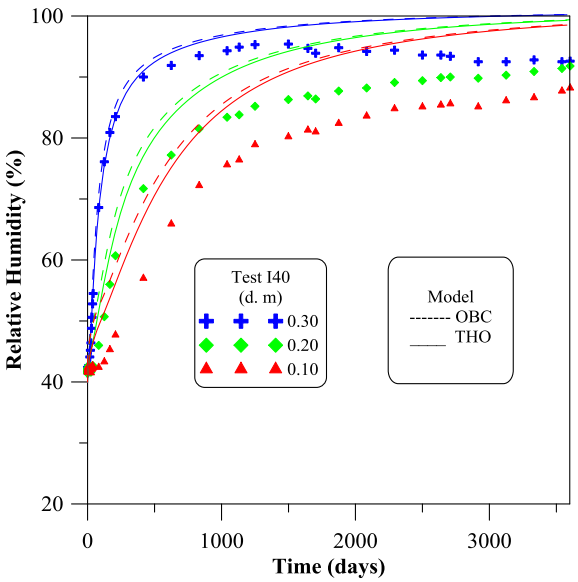

Figure 8: Evolution of Relative Humidity for the I40 Test: Experimental Data (scatter points) and Model Predictions up to 3600 days (10 years) for the (THO) and (OBC) cases at 0.30 m, 0.20 m and 0.10 m from the bottom of the cell.

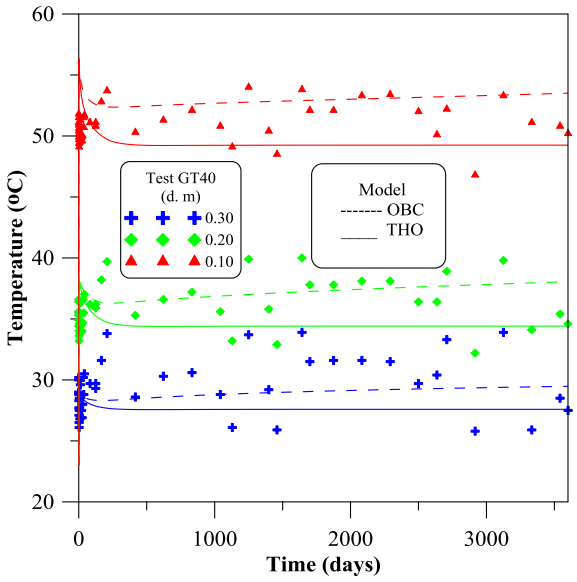

.

Figure 9. Evolution of Temperature for the GT40 Test: Experimental Data (scatter points) and Model Predictions up to 3600 days (10 years) for the (THO) and (OBC) cases at 0.30 m, 0.20 m and 0.10 m from the bottom of the cell.

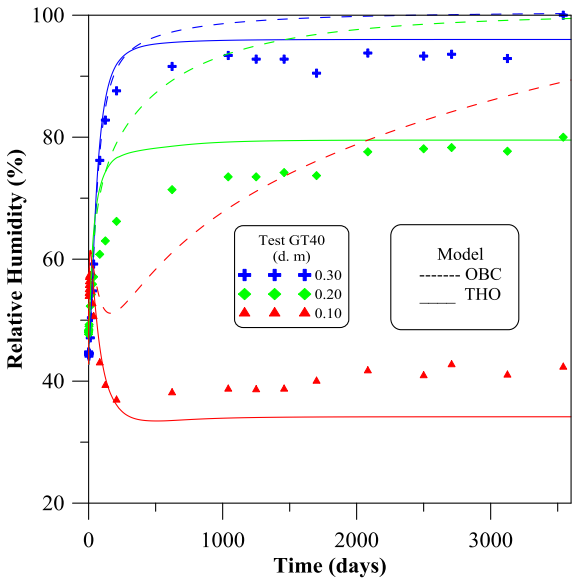

.

Figure 10. Evolution of Relative Humidity for the GT40 Test: Experimental Data (scatter points) and Model Predictions up to 3600 days (10 years) for the (THO) and (OBC) cases at 0.30 m, 0.20 m and 0.10 m from the bottom of the cell.

Table 1. Heat flux imposed at the top and bottom boundariesof the elements modeling the stored nuclear waste.

Storage Period (years)	Surface Heat Power ($W.m^{-2}$)	Relative Heat Power (%)
0 - 5	2.5.000	100.0
5 - 10	2.103	84.1
10 - 15	1.875	75.0
15 - 20	1.708	68.3
20 - 30	1.563	62.5
30 - 50	1.310	52.4
50 - 70	0.973	38.9
70 - 100	0.758	30.1
100 - 300	0.600	24.0
300 - 500	0.250	10.0
500 - 1000	0.125	5.0

(6)

Table 2. Main Model Parameters Used in the Simulation of Thermo-Osmotic Flow in Pollock's Problem of Nuclear Waste Storage.

k_T [$m^2.s^{-1}.°C^{-1}$]	k_{l0} [$m.s^{-1}$]	c_g [m^2]	P_o [Pa^{-1}]	n [-]
$5*10^{-11}$	$5*10^{-13}$	$5*10^{-12}$	10^{-4}	1.361
$_s$ [$W.m^{-1}.°C^{-1}$]	λ_l [$W.m^{-1}.°C^{-1}$]	λ_g [$W.m^{-1}.°C^{-1}$]	$_{vap}$ [$W.m^{-1}.°C^{-1}$]	
1.0500	0.6000	0.0258	0.011	
C_s [$J.kg^{-1}.°C^{-1}$]	C_w [$J.kg^{-1}.°C^{-1}$]	C_a [$J.kg^{-1}.°C^{-1}$]	C_{vap} [$J.kg^{-1}.°C^{-1}$]	h_{fg} [$J.kg^{-1}$]
837	4184	1000	1900	$2.5*10^{-6}$

Table 3. Main parameters of the OBC model

Equation	Variable name	Equation	Parameter relationships	Parameters
Constitutive equations				
Darcy' laws	Liquid and gas advective flux	$\mathbf{q}_l = -\mathbf{k}\ \frac{k_{rl}}{\mu_l}\left(\nabla P_l - \rho_l \mathbf{g}\right)$	$\mathbf{k} = k_0 \frac{n^3}{(1-n)^2}\frac{(1-n_0)^2}{n_0^3}\mathbf{I} \quad k_{rl} = S_e^{n_s}$	k_0=1.9 e^{-21} m^2; n_0 = 0.40; n_s = 3
Fick's law	Vapor non advective flux	$\mathbf{i}_g^w = -\ \left(n\rho_g S_g \tau D_m^w \mathbf{I} + \rho_g \mathbf{D}_g^{'}\right)\ \nabla \omega_g^w$	$D_m^w = 5.9x10^{-12}\frac{(273.15+T)^{2.3}}{P_g}$	τ =0.8
Fourier's law	Conductive heat flux	$\mathbf{i}_c = -\lambda \nabla T$	$\lambda = \lambda_{sat}^{s_e}\lambda_{dry}^{(1-s_e)}$	λ_{sat}=1.15 λ_{dry}=0.47
Retention curve	Phase degree of saturation	$S_e = \left[1+\left(\frac{s}{P_o}\right)^{\frac{1}{1-\lambda_o}}\right]^{-\lambda_o}\left(1-\frac{s}{P_d}\right)^{\lambda_d}$	$S_e = \frac{S_l - S_{lr}}{S_{ls}-S_{lr}} \qquad S_l = 1 - S_g$	P_0=28 MPa; λ=0.18 P_d=1100MPa; λ_d=1.1
Mechanical Constitutive Model	Stress Tensor	$\dot{\boldsymbol{\sigma}} = \mathbf{D}_{ep}\cdot\dot{\boldsymbol{\varepsilon}} + \boldsymbol{\gamma}_s \dot{s} + \boldsymbol{\gamma}_T \dot{T}$; $\frac{\dot{p}_0^*}{p_0^*} = \frac{(1+e)}{(\lambda_{(0)}-\kappa)}\dot{\varepsilon}_v^p$ $\dot{\varepsilon}_v^e = \frac{\kappa}{(1+e)}\frac{\dot{p}}{p} + \frac{\kappa_s}{(1+e)}\frac{\dot{s}}{(s+0.1)} + (\alpha_0 + \alpha_2\Delta T)\dot{T}$	$F = \frac{3J^2}{g_y^{\ 2}} - L_y^{\ 2}(p+P_s)(P_o - p) = 0$; $p_0 = p_c\left(\frac{p_{0T}^*}{p_c}\right)^{\frac{\lambda_{(0)}-\kappa}{\lambda_{(s)}-\kappa}}$ $p_s = k s\ e^{-\rho\Delta T}$; $p_{0T}^* = p_0^* + 2\left(\alpha_1\Delta T + \alpha_3\Delta T\lvert\Delta T\rvert\right)$ $\lambda_{(s)} = \lambda_{(0)}\left[r + (1-r)\exp(-\zeta s)\right]$ Mechanical model from Alonso et al. (1990) & Gens (1995)	κ=0.04; $\lambda_{(o)}$=0.14 P_o^*=14 MPa r=0.75; ζ=0.05 p_c=0.10MPa; M=1.5 k=0.1; ν=0.4 α_1=1.5x10^{-4} [1/C]; ρ=0.2 κs=0.25; α_{is}=-0.003
Phase density	Liquid density Gas density	$\rho_l = 1002.6\exp\left(4.5x10^{-4}(P_l - 0.1) - 3.4x10^{-4}T\right)$; ρ_g= ideal gas law		
Phase viscosity	Liquid viscosity Gas viscosity	$\mu_l = 2.1x10^{-12}\exp\left(\frac{1808.5}{273.15+T}\right)$; $\mu_g = 1.48x10^{-12}\exp\left(\frac{(273.15+T)^{1/2}}{1+\frac{119}{(273.15+T)}}\right)$		
Equilibrium restrictions				
Henry's Law	Air dissolved mass fraction	$\theta_l^a = \omega_a^l \rho_l = \frac{P_a}{H}\frac{M_a}{M_w}\rho_l$		
Psychometric Law	Water vapour dissolved mass fraction	$\theta_g^w = \left(\theta_g^w\right)^0 \exp\left(\frac{\Psi M_w}{R(273.15+T)\rho_l}\right)$	$\left(\theta_g^w\right)^0 = \frac{M_w P_{v(T)}}{R(273.15+T)}$	